Green Chemistry

PAPER

View Article Online
View Journal

Cite this: DOI: 10.1039/d5gc05411g

Electrochemical selective recovery of thorium from rare earths using an amidoxime modified graphite felt electrode

Peilin Lei,[a,b,c,d] Yun Gao[a,b] and Xiaoqi Sun *[a,b,c,d]

Received 11th October 2025,
Accepted 16th December 2025

DOI: 10.1039/d5gc05411g

rsc.li/greenchem

Thorium (Th) is a natural radioactive element often associated with rare earths. The efficient recovery of Th is not only essential for environmental protection, but also facilitates its potential reuse as a nuclear fuel. A graphite felt electrode modified with amidoxime (GF-AO) was synthesized for the electrochemical recovery of Th in this study. The GF-AO electrode demonstrated a high recovery capacity and excellent selectivity towards Th. Under the action of an electric field between the electrodes, the selectivity of separation between Th and rare earths was significantly improved. The physical and chemical recovery capacity of the GF-AO electrode for Th was 121.51 mg g^{-1}, while its electrochemical recovery capacity reached 3431 mg g^{-1}. The excellent capacity and selectivity of the GF-AO electrode provides a new approach for the green and efficient recovery of Th.

Green foundation

1. Thorium (Th) is a natural radioactive element often associated with rare earths. The efficient separation and recovery of Th is not only essential for environmental protection, but also facilitates its potential reuse as a valuable nuclear fuel resource.
2. Toxic and volatile organic solvents are typically involved in Th extraction, posing secondary pollution risks. This electrochemical recovery does not require organic solvents, demonstrating excellent recovery ability and selectivity for Th.
3. In future work, the electrochemical recovery method is expected to be coupled with renewable energy such as solar power and wind power, supporting the development of green and efficient recycling technologies for critical metals.

Introduction

Rare earth elements (REEs) are indispensable strategic resources in modern industry, with widespread applications in semiconductors, ceramics, phosphors, and emerging energy technologies.[1,2] However, due to their similar physicochemical properties, Th often co-occurs with REEs in mineral deposits, resulting in its presence in both leachates and solid residues from REE separation processes.[3,4] Th is a naturally radioactive element with high environmental mobility and bioaccumulation potential. Improper disposal of Th can pose significant risks to both environmental and human health.[5,6] Therefore, the efficient separation and recovery of Th is not only essential for environmental protection, but also facilitates its potential reuse as a valuable resource.[7,8]

Th is regarded as a promising nuclear fuel for next-generation nuclear power systems, owing to its favourable nuclear properties and economic advantages.[9,10] Th-based reactors are considered a potential direction for the future of nuclear energy. Therefore, it is expected that the demand for Th will increase.[11,12] Given the substantial Th content in rare earth ores and industrial residues, its recovery holds considerable promise.[13,14] Currently, solvent extraction is the dominant method for Th separation.[15,16] However, it typically involves toxic and volatile organic solvents in the separation process, posing secondary environmental pollution risks.[4,17] In contrast, solid-phase adsorbents offer a more sustainable and cost-effective alternative, particularly suitable for the separation of radioactive Th ions from low-concentration wastewater.[18,19]

Although various adsorbents including metal sulfides, metal–organic frameworks (MOFs),[20–22] covalent organic frameworks (COFs),[23–26] and graphene-based materials[27,28] have demonstrated some degree of Th uptake, conventional adsorption methods often suffer from slow ion diffusion and limited adsorption capacity.[29,30] Electrochemical recovery has

[a]Fujian Institute of Research on the Structure of Matter, Chinese Academy of Sciences, Fuzhou, Fujian 350002, P. R. China. E-mail: xqsun@fjirsm.ac.cn
[b]Fujian Research Center for Rare Earth Engineering Technology, Xiamen Institute of Rare Earth Materials, Haixi Institute, Chinese Academy of Sciences, Xiamen, 361021, P. R. China
[c]University of Chinese Academy of Sciences, Beijing, 100039, P. R. China
[d]Fujian College, University of Chinese Academy of Sciences, Fuzhou, Fujian 350002, P. R. China

emerged as a superior strategy due to its enhanced adsorption kinetics and higher capacity.[31–34] While functionalized materials exhibit good selectivity toward Th, their traditional adsorption capacities remain low.[35–37] Recent studies have shown that electrochemical techniques can significantly improve the performance of amidoxime-based adsorbents.[38–40] The adsorption capacity of uranium extracted from seawater was increased from 200 mg g^{-1} to 1932 mg g^{-1} through electrochemical adsorption. The outstanding effect of this method also indicates its potential in Th recovery.[39]

Experimental

Chemicals and materials

Polyacrylonitrile (molecular weight 15 000, 99.00%) was purchased from Damas-beta. Hydroxylamine hydrochloride (99%), graphite felt (carbon content 99.9%) and ethanol (purity 99%) were obtained from Xilong Scientific. Conductive carbon black (carbon content 99.9%), *N*,*N*-dimethylformamide (99.5%) and nitric acid (68%) were also supplied by Xilong Chemical. Thorium nitrate [$Th(NO_3)_4$, 99% purity] was used as the Th source. Rare earth nitrate solutions were prepared by dissolving the corresponding rare earth oxides (REO, 99.99% purity) in nitric acid. Sodium hydroxide (99.9%) was purchased from China National Pharmaceutical Group Chemical Reagent Co., Ltd. All the reagents used were of analytical grade without further purification.

Material preparation

Graphite felt was immersed in 1 mol L^{-1} HCl and ultrasonically cleaned for 30 min. It was then rinsed three times with deionized water to remove the residual acid, followed by ethanol washing. The cleaned felt was dried in a 70 °C oven for 12 h. Polyacrylonitrile (PAN) and conductive carbon black were mixed in a 9 : 1 mass ratio. One gram of the mixture was dissolved in 50 mL DMF and stirred for 12 h to form a homogeneous slurry. The slurry was coated onto dried graphite felt and ultrasonicated to enhance penetration into the carbon fibers. The felt was dried at 80 °C for 12 h, and the coating process was repeated three times to obtain PAN-coated carbon felt (GF-CN). The final loading of PAN in GF-CN was 5.25 mg cm^{-2}. The CF-CN carbon felt was immersed in a 1 mol L^{-1} hydroxylamine hydrochloride solution. The solution was heated in a water bath to 70 °C, and a 1 mol L^{-1} sodium carbonate solution was slowly added dropwise. During this preparation process, the nitrile groups in the PAN were reduced to amidoxime groups over the course of 2 h. The modified felt was then rinsed thoroughly with deionized water to remove residual salts and dried in a hot-air oven at 70 °C for 12 h to yield the amidoxime-functionalized carbon felt, referred to as GF-AO.[38,41]

Characterization of electrode materials

The Th and REE ion concentrations before and after electrochemical recovery were measured using an inductively coupled plasma optical emission spectrometer (ICP-OES, Horiba ULTIMA, HORIBA, Japan). Solution pH was determined using a PHSJ-4F pH meter and adjusted to the desired value with NaOH or HNO_3. Electrochemical performance characterization and power input for the recovery process were carried out using a Princeton Applied Research V-200 electrochemical workstation. Fourier transform infrared (FTIR) spectra of the synthesized materials were recorded in the range of 500–4000 cm^{-1} using a spectrometer (Nicolet iS50). Changes in solution pH during the recovery process were continuously monitored using a Leici pH meter. Morphological analysis before and after recovery, along with elemental mapping of the electrode surface, was performed using a field-emission scanning electron microscope (FE-SEM, Apreo S LoVac, Thermo Fisher Scientific) equipped with an energy-dispersive X-ray spectroscopy (EDS) system. The contact angle of the synthesized materials was measured using a JY-PHb contact angle goniometer.

Recovery experiments

All the recovery experiments were conducted in a 50 mL electrochemical cell using a three-electrode setup. An amidoxime-functionalized graphite felt (1.5 × 1.5 cm^2) served as the working electrode, while a platinum sheet of the same size was used as the counter electrode, positioned 1 cm apart from the working electrode. A saturated Ag/AgCl electrode was used as the reference electrode. Th solutions with varying concentrations (10–1000 mg L^{-1}) and pH values (1–3) were added to the electrochemical cell. A Princeton Applied Research V200 power supply was used to apply either constant voltage or fast electrical pulse modes. The voltage was set between 0 V and −3 V, with pulse frequencies ranging from 100 to 1000 Hz and duty cycles from 0.2 to 1. The recovery capacity and removal efficiency were calculated using eqn (1) and (2), while the distribution coefficient (K_d, mL g^{-1}) and separation factor (SF) were determined using eqn (3) and (4).

$$Q = \frac{(C_0 - C_t)V}{m} \quad (1)$$

$$R = \frac{(C_0 - C_t)}{C_0} \times 100\% \quad (2)$$

$$K_d = \frac{(C_0 - C_t) \times V}{C_t \times m} \quad (3)$$

$$SF_{1/2} = \frac{K_{d1}}{K_{d2}}. \quad (4)$$

Infrared transmission analysis

Polyacrylonitrile-coated graphite felt and amidoxime-functionalized graphite felt were ground into fine powders using an agate mortar. The powders were then uniformly mixed with spectroscopic-grade potassium bromide (KBr), pressed into pellets using a hydraulic press and formed into KBr windows for FTIR transmission measurements. As shown in Fig. 1, the infrared transmission spectra clearly show the characteristic stretching vibration peak of the nitrile (–CN) group in polyacry-

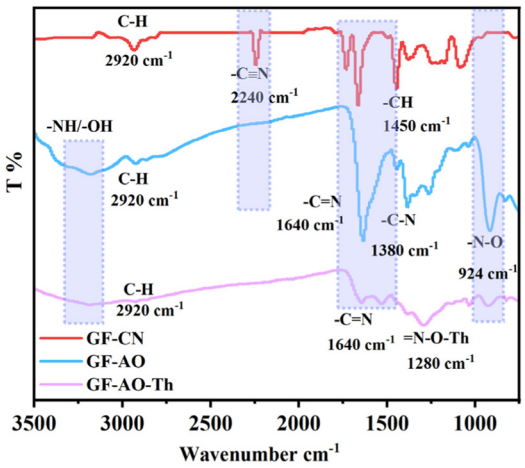

Fig. 1 FT-IR spectra of GF-CN, GF-AO and GF-AO-Th.

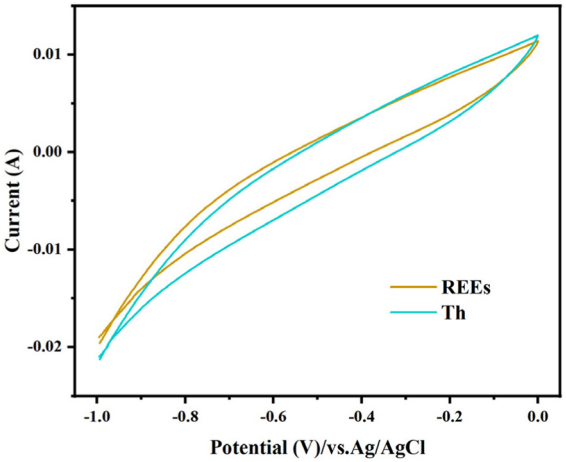

Fig. 2 CV of GF-AO for Th and REEs.

lonitrile at 2240 cm^{-1}. This peak disappears after treatment with hydroxylamine hydrochloride, confirming the complete reduction of –CN groups. In the spectrum of the amidoxime-functionalized sample (GF-AO), a new peak appears at 1640 cm^{-1}, corresponding to the C=N stretching vibration of the amidoxime group.[42,43] Another characteristic peak at 924 cm^{-1} is attributed to the N–O stretching vibration. Additionally, broad absorption bands above 3000 cm^{-1} are associated with –NH and –OH stretching vibrations of the amidoxime moiety. These results indicate that the nitrile groups in GF-CN were successfully converted to amidoxime groups by hydroxylamine treatment.[44,45] As can be seen in GF-AO and GF-AO-Th, the infrared spectra confirm the presence of strong interactions between Th and the oxygen atoms on the amidoxime groups, with pronounced changes observed in the amidoxime moieties following Th capture.

Electrochemical characterization

Cyclic voltammetry (CV) was used to evaluate the specific capacitance of ions on the electrode surface (Fig. 2). The concentrations of Th and REEs (Y, La, Ce, Pr, Nd, Sm, Eu, Gd, Tb, Dy, Ho, Er, Tm, Yb, Lu) were maintained at 1 mmol L^{-1}, pH was maintained at 2, the scan ratio was 100 mV s^{-1}, and the electrode potential was −1 V to 0 V (*vs.* Ag/AgCl). The electrodes exhibit different specific capacitances in different solutions. The GF-AO electrode exhibits a specific capacitance of 3.1 F g^{-1} in REE solution and 3.9 F g^{-1} in Th solution. The higher specific capacitance exhibited by Th confirms its superior capacity to form a double layer on the electrode, thereby demonstrating that Th is more effectively captured by the amidoxime groups immobilized on the electrode.

Scanning electron microscopy

The surface morphology and elemental composition of the electrode materials before and after recovery were examined using field-emission scanning electron microscopy (FE-SEM) and energy-dispersive X-ray spectroscopy (EDS) (Thermo Fisher Scientific Apreo S LoVac). The SEM images reveal distinct morphological changes on the surface of the graphite felt before and after modification. As shown in Fig. 3, the pristine graphite felt exhibits smooth and well-defined graphite fibers. After coating with polyacrylonitrile, the fiber surfaces are partially covered with particulate matter, attributed to the conductive carbon black and the polymer coating. After recovery, significant changes in surface morphology are observed on the amidoxime-functionalized electrode. A noticeable increase in fiber diameter is evident, likely due to the deposition of neutral thorium hydroxide on the graphite fibers. Before recovery, the carbon fibers appear smooth, while after recovery, they are coated with flake-like thorium hydroxide deposits. At the macroscopic level, the electrode surface changes from black (pre-recovery) to white (post-recovery), indicating coverage by the newly formed thorium hydroxide layer.

EDS characterization

Elemental distribution on the electrode surface before and after adsorption was analysed using the EDS system integrated

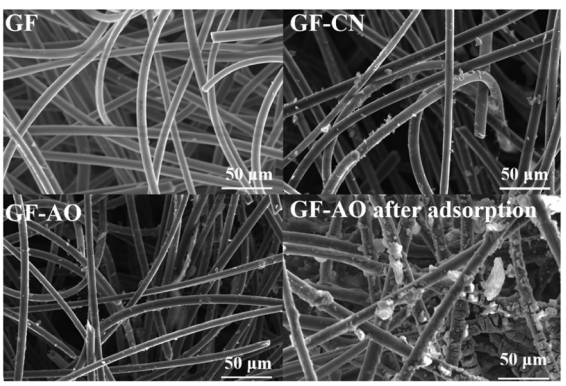

Fig. 3 SEM images of GF, GF-CN, GF-AO and GF-AO after Th adsorption.

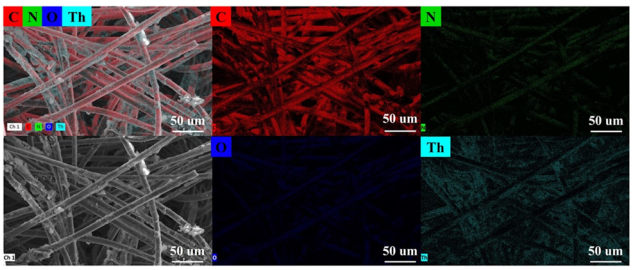

Fig. 4 EDS of GF-AO after Th adsorption.

with a scanning electron microscope. As shown in Fig. 4, a distinct Th signal can be detected after adsorption, confirming the presence of Th on the electrode surface. During the electrochemical adsorption process, Th ions were captured by amidoxime functional groups on the carbon felt surface. Concurrently, water electrolysis at the electrode caused a localized increase in pH near the adsorption site. This led to the formation of electrically neutral thorium hydroxide through the reaction with hydroxide ions, resulting in the deposition of Th species on the electrode surface.

Results and discussion

Adsorption performance of different materials

Three types of graphite felt, unmodified graphite felt (GF), polyacrylonitrile-coated graphite felt (GF-CN), and amidoxime-functionalized graphite felt (GF-AO) were used as electrodes for electrochemical adsorption in a 1000 ppm Th solution at a pH value of 2. A constant voltage of −1.5 V was applied for 12 h. As shown in Fig. 5a, the adsorption capacities of the different materials were calculated. Both GF and GF-CN exhibited similar adsorption capacities of 993.12 mg g^{-1} and 998.25 mg g^{-1}, respectively. In contrast, the amidoxime-functionalized graphite felt (GF-AO) demonstrated a significantly higher adsorption capacity of 1845.97 mg g^{-1}, attributed to the improved wettability and stronger interaction with Th ions. These results indicate that amidoxime functionalization substantially enhances the electrode's affinity for Th, enabling GF-AO to achieve superior adsorption performance.

Effect of voltage on adsorption

The applied voltage plays a crucial role in the adsorption performance of the electrode. In the electrochemical cell, 50 mL of thorium nitrate solution (with an initial concentration of 1000 ppm and a pH value of 2) was used as the adsorbate. A 1.5 × 1.5 cm^2 graphite felt electrode was employed as the working electrode, and a constant voltage ranging from −3 V to 0 V (relative to a saturated silver chloride reference electrode) was applied for 12 h of Th recovery. In static recovery, no voltage was applied and other factors were kept the same as in the electrochemical recovery process. As shown in Fig. 5b, the amidoxime-modified graphite felt (GF-AO) exhibi-

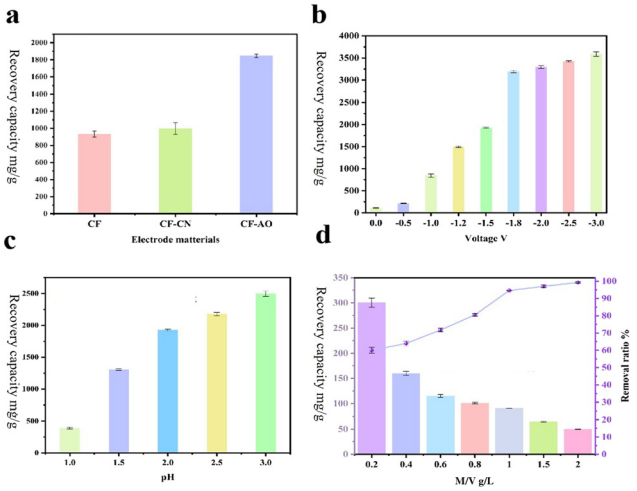

Fig. 5 (a) Effect of voltage on Th recovery with different electrodes. (b) Effect of the voltage. (c) Effect of pH on Th adsorption with a constant DC voltage of −1.5 V, an initial Th concentration of 1000 ppm, pH = 2. (d) Effect of mass-to-liquid pH = 2, constant DC voltage of −1.5 V.

ted a recovery capacity of 843.51 mg g^{-1} when a voltage of −1 V was applied, significantly higher than the 121.51 mg g^{-1} obtained under static conditions. This indicates that the electric field between the electrodes accelerates the migration of Th ions to the electrode surface, increasing the contact probability between Th ions and the recovery material. Additionally, the Th ions adsorbed on the electrode can be neutralized by OH^- ions near the electrode, promptly releasing recovery active sites, thereby enhancing the electrode's recovery capacity. As the applied voltage is increased, the recovery capacity is also increased. The electric field between the electrodes drove the formation of a thicker electric double layer (EDL) on the electrode surface, promoting the recovery of Th. With increasing voltage, the electric field force was intensified, accelerating the migration rate of ions between the electrodes and increasing the accumulation of Th ions on the electrode surface. At −3 V, the GF-AO electrode achieved a recovery capacity of 3586 mg g^{-1}. However, water decomposition at the electrode led to an increase in current when the applied voltage exceeded the theoretical decomposition voltage of water and the polarization voltage required for water splitting. Consequently, the current density on the electrode increased. To minimize energy consumption during the recovery process, −1.5 V was chosen as the recovery voltage for subsequent investigation.

Effect of pH on recovery

pH value is one of the key factors influencing the electrochemical recovery of Th. This study investigates the effect of pH value on the recovery of Th ions within a concentration of 1000 ppm (C_0) and a pH range of 1 to 3. To prevent hydrolysis of Th ions at higher pH levels, the pH of the solution was controlled to remain below 3, preventing the precipitation of Th $(OH)_4$ in solutions with higher pH. A constant voltage of −1.5

V was applied to the working electrode for 12 h during the recovery process. As shown in Fig. 5c, the recovery capacity of the amidoxime functionalized graphite felt (GF-AO) increases as the pH of the solution rises. At lower pH, the recovery of Th by the electrode material is relatively low, as the H^+ ions in the solution strongly compete with Th and inhibit the recovery of Th. At lower pH values, H^+ ions tend to compete for recovery sites on the electrode, which may also lead to the re-dissolution of thorium hydroxide adsorbed on the electrode into the solution. At the pH value of 1.0, the recovery capacity of the electrode for Th was 400.85 mg g^{-1}. In solutions with low pH, the local pH increase caused by water electrolysis near the electrode is minimal. However, the increase in local pH due to water electrolysis is more significant in solutions with higher pH, which helps to neutralize the Th(IV) adsorbed on the electrode, forming neutral thorium hydroxide. The recovery capacity of Th increases significantly as the pH of the solution rises. The increase in local pH near the electrode leads to the neutralization of Th ions at higher pH, forming thorium hydroxide and releasing more active recovery sites. Additionally, the adsorbed Th(IV) on the electrode is less likely to be dissolved and re-enter the solution due to the reduced presence of H^+ ions in higher pH solutions. At the pH value of 3, the recovery capacity of Th reaches 2595.42 mg g^{-1}.

Effect of solid-to-liquid ratio (m/v) on recovery

The ratio of electrode mass to solution volume is a critical factor influencing the removal efficiency of Th ions. As shown in Fig. 5d, to improve Th removal from high-concentration solutions, a series of electrochemical recovery experiments were conducted at an initial Th concentration of 50 ppm and a pH value of 3. Different solid-to-liquid ratios such as 0.2, 0.4, 0.6, 0.8, 1.0, 1.5, and 2.0 g L^{-1} were tested. A constant voltage of −1.5 V was applied to the working electrode for 8 h. The results show that increasing the solid-to-liquid ratio significantly enhanced the Th removal efficiency. When the ratio exceeded 1 g L^{-1}, the removal rate of Th surpassed 95%. This demonstrates that a higher electrode loading relative to solution volume facilitates more effective Th extraction.

Effect of initial concentration on recovery

As shown in Fig. 6a, electrochemical recovery experiments were conducted at pH = 2 with varying initial Th concentrations (C_0 = 10, 50, 100, 200, 300, 400, 500, and 1000 ppm). A constant voltage of −1.5 V was applied to the working electrode for 12 h. The recovery capacity of the electrode increased with the initial concentration of Th. At lower Th concentrations, the recovery capacity was relatively low due to limited availability of Th(IV). As the initial concentration was increased, more Th ions were available to interact with the recovery sites on the electrode, leading to higher recovery capacities. Specifically, the recovery capacity was 28.76 mg g^{-1} when C_0 was 10 ppm. When C_0 was 100 ppm, the recovery capacity of Th increased to 197.98 mg g^{-1}. Further increasing the Th concentration to 500 ppm resulted in a recovery capacity of 709.33 mg g^{-1}. At the highest Th tested concentration of 1000 ppm, the electrode

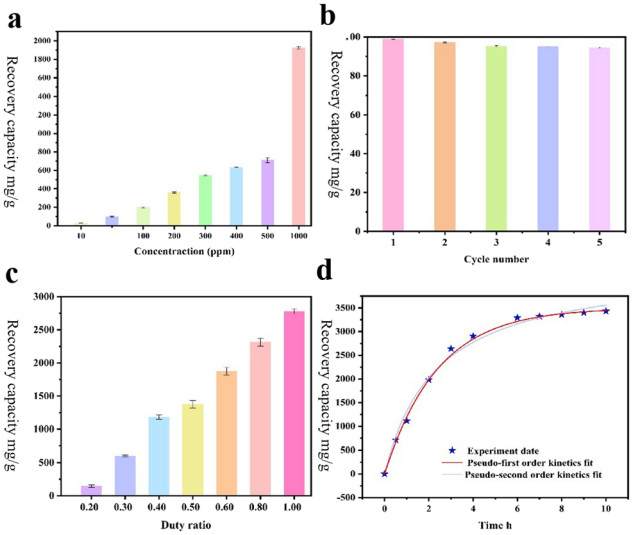

Fig. 6 (a) Effect of initial concentration of Th recovery with different electrodes. (b) Reusability of the electrode material. (c) Effect of duty cycle on Th recovery, initial Th concentration is 1000 ppm, pH = 2. (d) Recovery kinetics.

achieved a maximum Th recovery capacity of 1925.75 mg g^{-1}. These results indicate that the recovery process was highly dependent on the initial concentration of Th ions in the solution.

Reusability of the electrode material

The recyclability of the adsorbent is a key factor in evaluating its practical performance, as repeated use can significantly reduce operational costs and enhance the economic viability of recovery-based methods. To assess the reusability, the electrode was immersed in a solution containing 50 ppm Th at the pH value of 3. A constant voltage of −2 V was applied to the working electrode, and each recovery cycle lasted for 8 h. As shown in Fig. 6b, the electrode after Th recovery was regenerated by soaking in 0.1 mol L^{-1} nitric acid for 2 h to desorb the Th, followed by neutralization in 0.2 mol L^{-1} sodium carbonate solution to remove excess acid from the surface. The electrode was then rinsed with flowing deionized water until the rinse solution reached neutral pH and subsequently dried at 70 °C to complete the regeneration process. The electrode exhibited an initial Th removal efficiency of 98.94%. After five adsorption–desorption cycles, the removal efficiency remained above 95%, demonstrating excellent stability and reusability of the electrode material.

Effect of duty cycle on recovery

The duty cycle is a critical parameter in electrochemical recovery, especially when applying pulsed power in separation experiments to enhance the Th/REE ion selectivity. The duty cycle refers to the ratio of the "on-time" to the total duration of a single pulse cycle. In these experiments, the electrode potential was set to −3 V during the on-time and 0 V during the off-time. As shown in Fig. 6c, a series of tests were conducted to evaluate the effect of varying duty cycles 0.2, 0.4, 0.6, 0.8, and

1.0 (corresponding to continuous DC power) at a pulse frequency of 400 Hz. Th recovery was carried out in a 1000 ppm $Th(NO_3)_4$ solution at pH = 2. As shown in Fig. 6d, the total energized time for all experiments was maintained at 4 h to ensure comparability. At low duty cycles, the recovery capacity was significantly lower. For example, at a duty cycle of 0.2, the recovery capacity was only 158.85 mg g^{-1}, slightly above that of static (non-electric) recovery. This was attributed to the longer off-time within each pulse cycle, during which adsorbed Th ions could be diffused away from the electrode surface and redissolved into the solution under the influence of H^+ ions. As the duty cycle was increased, the off-time was shortened, reducing the likelihood of Th desorption. At a duty cycle of 0.3, the recovery capacity increased to 600.35 mg g^{-1}. When the duty cycle exceeded 0.6, desorption during the off-time became negligible, allowing more ions to remain adsorbed and be captured in subsequent cycles. This resulted in a significantly higher capacity of 1875.65 mg g^{-1}. When the duty cycle exceeded 0.8, the recovery performance approached that of constant DC operation, with the electrode capturing up to 2313.12 mg g^{-1} of Th. Under continuous DC voltage (duty cycle = 1.0), the maximum Th recovery capacity reached 2778.18 mg g^{-1}. This demonstrates that higher duty cycles are more effective for electrochemical recovery by minimizing ion desorption and maximizing retention at the electrode surface.

Recovery kinetics

The electrode material exhibits rapid recovery kinetics. In a solution with an initial Th ion concentration of 1000 ppm and pH = 2, a constant voltage of −3 V was applied to the recovery electrode. As shown in Fig. 6d, the recovery capacity reached 3431 mg g^{-1} after 10 h of electrochemical recovery. Within the first 30 min, the electrode had already adsorbed 710.44 mg g^{-1} of Th ions and the capacity was increased to 1114.32 mg g^{-1} after 1 h. Over the full 10 h period, the final recovery capacity reached 3431 mg g^{-1}.

Effect of applied voltage on selective recovery

The GF-AO electrode was immersed in a mixed solution with an initial pH of 1.5, containing both Th and REE ions at equal initial concentrations of 1 mmol L^{-1}. Pulsed electrochemical recovery was applied using a square wave pulse with a frequency of 400 Hz and a duty cycle of 0.3, aiming to selectively separate Th from competing REE ions by screening different applied voltages. As shown in Fig. 7a, the recovery time was kept identical to the duration of energized pulsing in the static recovery control (no voltage applied). Th removal was only 8.78% under these conditions, indicating that purely physical or chemical recovery has limited selectivity and efficiency. Applying a pulsed voltage of −1.5 V increased Th removal to 22.91%, demonstrating that the electric field significantly enhances Th(IV) migration toward the electrode surface. However, the performance at this voltage and duty cycle remained suboptimal. To further improve Th removal, the applied voltage was increased. At the voltage of −2 V, the Th removal rate rose modestly to 29.19%. When the pulsed voltage was increased to −3 V, Th removal reached a significantly higher value of 89.11%, maintaining good selectivity over REE ions. Therefore, a pulse voltage of −3V and a duty cycle of 0.3 were used as the optimal operating conditions in the subsequent experiment of selective electrochemical recovery of Th.

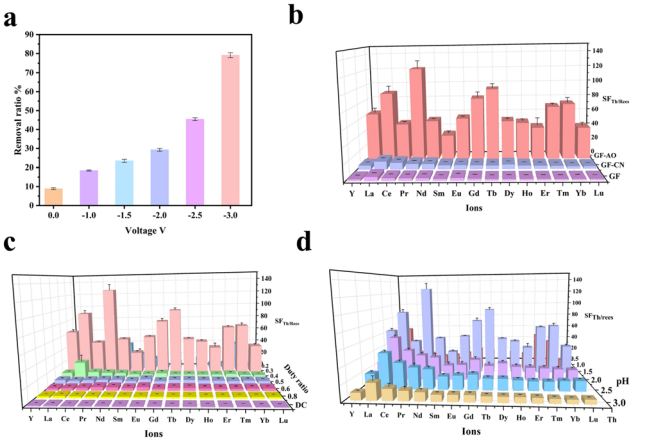

Fig. 7 (a) The effect of voltage on the separation factor, pH = 1.25, voltage −3 V, and frequency 100 Hz. (b) The effect of different electrodes on the separation factor, pH = 1.5, voltage −3 V, frequency 400 Hz, duty ratio 0.3. (c) The effect of duty cycle on the separation factor, pH = 1.5, duty ratio 0.3, voltage −3 V. (d) The effect of pH on the separation factor, pH = 1.5, voltage −3 V, frequency 400 Hz, duty ratio 0.3.

Selective recovery performance of different electrodes

To demonstrate that GF-AO is the key to achieving selective electrosorption of Th, three types of graphite felt electrodes GF, GF-CN, and GF-AO were immersed in a mixed solution containing equal concentrations (1 mmol L^{-1}) of Th and rare earth ions at the pH value of 1.5. A pulsed electric field (−3 V, 100 Hz, duty cycle 0.3) was applied to the electrodes to assess their selectivity toward Th over REEs. The GF exhibited no significant selectivity with a separation factor close to 1 as shown in Fig. 7b, adsorbing Th and rare earth ions at nearly equal levels under pulsed potential. Similarly, the GF-CN electrode showed only weak selectivity, with a separation factor below 10. In contrast, the GF-AO electrode demonstrated both high recovery capacity and excellent selectivity for Th. Under pulsed electric field conditions, GF-AO enabled preferential recovery of Th while minimally adsorbing REE ions, even in the presence of equimolar concentrations of multiple competing ions. The high separation factor between Th and REE ions confirms that the amidoxime functional groups on GF-AO play a crucial role in selective recovery. These results highlight the significance of surface functionalization with amidoxime groups in enhancing the selectivity of electrode materials for Th in competitive environments.

Effect of duty cycle on selectivity

The duty cycle is a critical factor influencing the separation performance of electrode materials. Herein, a simulated solu-

tion with a pH value of 1.5 and a metal concentration of 1 mM was used. A pulsed voltage of 3 V at 100 Hz was applied, with duty cycles set to 0.2, 0.3, 0.5, 0.6, 0.8, and 1.0 (continuous DC voltage). As shown in Fig. 7c, the longer diffusion time in each pulse cycle allows previously adsorbed Th ions to be redissolved into the solution when the duty cycle is 0.2. Although the total energized time was constant across experiments, the extended off-time at lower duty cycles allowed more desorption, resulting in low overall recovery for both Th and REE ions on the GF-AO electrode. As the duty cycle was increased, the recovery capacity for Th was improved significantly and the electrode demonstrated greater selectivity for Th. This improvement is attributed to the optimal balance between the ion migration time toward the electrode and the diffusion time for desorbing competing ions within each pulse cycle. When the duty cycle exceeded 0.6, the energized period within each cycle became dominant. This limited the diffusion of competing ions away from the electrode surface, leading to their recovery in the subsequent cycles. At a duty cycle of 1.0 (continuous DC), selectivity was lost entirely. The constant electric field continuously drove both Th and competing REE ions to the electrode, resulting in non-selective recovery. This is due to the reduced diffusion interval at high duty cycles, where adsorbed metal ions, including non-target ions, had insufficient time to diffuse back into the bulk solution before being re-adsorbed in the next cycle. Among all tested conditions, a duty cycle of 0.3 provided the best balance, enabling the GF-AO electrode to achieve optimal selectivity for Th over REE ions.

Effect of pH on selective recovery

The pH of the solution is a critical factor influencing the selective recovery of Th by the electrode material. In this study, mixed solutions containing equimolar concentrations (1 mmol L^{-1}) of Th and a full suite of REEs were prepared at varying pH levels of 1.25, 1.5, 2.0, 2.5, and 3.0. A pulsed electric field (−3 V, 400 Hz, duty cycle 0.3) was applied to the working electrode during recovery. As shown in Fig. 7d, the high concentration of H^+ in the solution leads to the re-dissolution of thorium hydroxide adsorbed on the electrode surface at lower pH levels. Additionally, protons compete with Th(IV) for recovery sites on the electrode, resulting in a lower Th uptake. As the pH increases, the recovery capacity for Th improves, and the electrode exhibits better selectivity toward Th over REEs. In the solution with a low pH value, the local increase in pH value near the electrode during the recovery process is limited. In contrast, the local pH rise near the electrode is more pronounced, leading to a higher hydroxide ion concentration which promotes the formation of thorium hydroxide and enhances Th recovery. However, REE ions also begin to form insoluble hydroxides that remain on the electrode surface as the pH value is increased. These precipitates do not readily redissolve, causing both Th(IV) and REE(III) adsorptions to increase thereby reducing the electrode's selectivity for Th. While a moderately acidic environment enhances selective recovery of Th(IV), excessively high pH levels lead to co-recovery of REE ions, diminishing the electrode's selectivity.

Selectivity of the GF-AO electrode

Under optimal conditions, the CF-AO electrode after adsorption was immersed in an equal volume of 0.1 mol L^{-1} dilute nitric acid for desorption. The desorbed solution was then diluted and analysed using ICP-OES to determine the concentration of each ion. Electrochemical recovery effectively enriches and separates Th from REEs. As shown in Fig. 8, the Th concentration reaches as high as 125.24 ppm. Thanks to the excellent selectivity of the GF-AO electrode, 125.24 mg g^{-1} adsorption capacity of Th is achieved while absorption of La is 0.35 mg g^{-1}, Ce is 0.52 mg g^{-1}, Pr is 0.46 mg g^{-1}, Nd is 0.53 mg g^{-1}, Sm is 0.87 mg g^{-1}, Eu is 0.66 mg g^{-1}, Gd is 0.65 mg g^{-1}, Tb is 0.60 mg g^{-1}, Dy is 0.71 mg g^{-1}, Ho is 0.64 mg g^{-1}, Er is 0.73 mg g^{-1}, Tm is 0.77 mg g^{-1}, Yb is 1.72 mg g^{-1}, Lu is 1.67 mg g^{-1}. The $SF_{Th/La}$ is 181.3, $SF_{Th/Ce}$ is 150.7, $SF_{Th/Pr}$ is 133.2, $SF_{Th/Nd}$ is 124.2, $SF_{Th/Sm}$ is 86.3, $SF_{Th/Eu}$ is 118.3, $SF_{Th/Gd}$ is 118.1, $SF_{Th/Tb}$ is 112.8, $SF_{Th/Dy}$ is 110.8, $SF_{Th/Ho}$ is 114.3, $SF_{Th/Er}$ is 112.7, $SF_{Th/Tm}$ is 108.3, $SF_{Th/Yb}$ is 61.2, and $SF_{Th/Lu}$ is 65.4, respectively. The concentrations of REE ions remained very low, with individual element concentrations not exceeding 5 ppm. This demonstrates that electrochemical recovery using the GF-AO electrode can selectively separate and enrich Th from REE mixtures, enabling efficient recovery and utilization of Th. The fundamental reason for this selectivity is that the charge density of Th(IV) is higher than that of REE(III), making it easier for the NOH functional group in oxime to coordinate with Th(IV). Therefore, the CF-AO electrode has better selectivity for Th(IV).

Mechanism investigation

The electrochemical Th adsorption apparatus is illustrated in Fig. 9. Under pulsed electric fields, the GF-AO electrode demonstrates excellent adsorption selectivity toward Th(IV) ions. The adsorption–separation mechanism can be summarized in five steps. In Step I, ions in the mixed solution are randomly distributed. Step II involves migration of cations and anions toward the working electrode under an applied voltage,

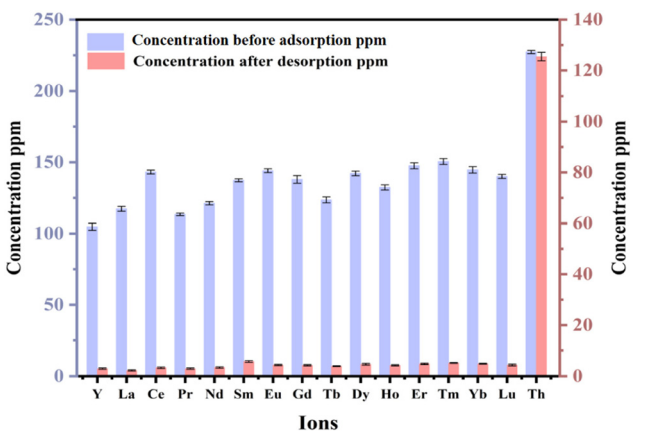

Fig. 8 The removal efficiency of the electrode for Th under optimal conditions.

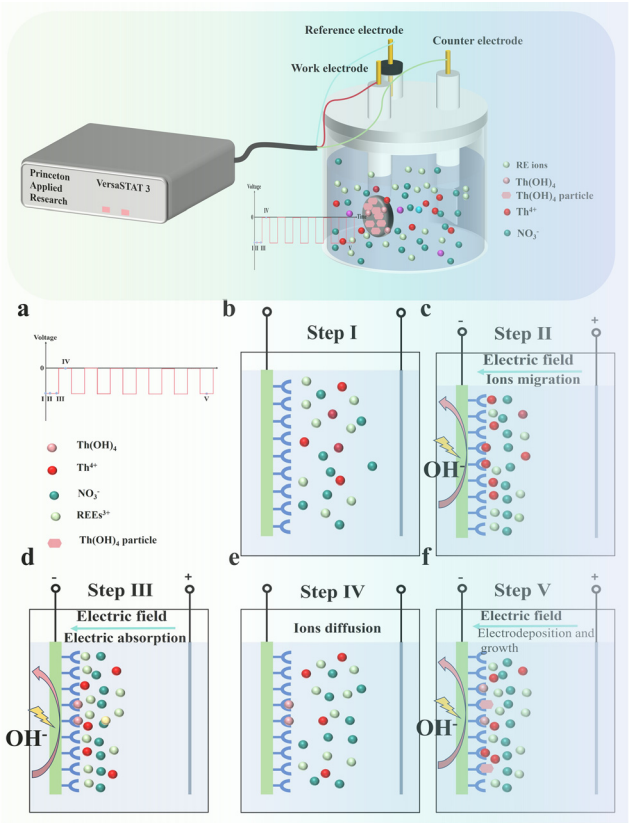

Fig. 9 Schematic figure of the selective Th adsorption process.

forming an electrical double layer (EDL), where Th(IV) ions are selectively adsorbed *via* coordination with amidoxime groups. In Step III, Th and competing ions are co-adsorbed; the adsorbed metal ions react with nearby OH^- to form neutral metal hydroxides on the electrode surface. Upon removal of the applied voltage in Step IV, competing ions are desorbed back into the solution due to their weak affinity for the amidoxime group. Th(IV) remains bound due to its stronger interaction, resulting in its enrichment on the electrode. Due to the desorption and diffusion of weakly bound ions back into the solution, active sites are regenerated. Finally, in Step V, Th(IV) continuously accumulates as thorium hydroxide at active sites, growing into particulate deposits and effectively enriching Th on the electrode surface. X-ray diffraction (PXRD) was used to characterize the electrode products as shown in Fig. S3, thereby confirming the presence of Th in the form of an amorphous hydroxide phase.

Conclusion

The amidoxime-functionalized graphite felt (GF-AO) electrode exhibits excellent recovery affinity for Th(IV), achieving a high recovery capacity and fast recovery ratio compared with other functional adsorbents and electrosorption methods as shown in Table S2. Even at lower applied voltages, the electrode maintains strong performance, with a recovery capacity of 2595.42 mg g^{-1} at pH 3. Lowering the recovery voltage effectively reduces both energy consumption and water electrolysis during the process. Even in the presence of competing ions, the GF-AO electrode demonstrates good selectivity for Th(IV) due to the strong affinity of the amidoxime groups. Using pulsed electric fields during recovery not only suppresses water electrolysis, but also promotes the desorption of REE ions from the electrode surface back into the bulk solution, enhancing the selectivity for Th. The GF-AO electrode maintains excellent performance even at low voltages, making it a more energy-efficient option. In addition, the electrode demonstrates good regeneration and cycling stability, which reduces the overall cost of Th recovery and enhances the economic viability of the process. Electrochemical recovery of Th greatly reduces the use of acids, bases, and organic solvents. In the future, it can be combined with renewable energy sources such as wind and solar power to achieve green and low-carbon recycling of Th.

Author contributions

Peilin Lei: methodology, formal analysis, investigation, visualization, and writing – original draft. Yun Gao: investigation, data curation, and formal analysis. Xiaoqi Sun: conceptualization, resources, supervision, writing – review & editing, and project administration.

Conflicts of interest

There are no conflicts to declare.

Data availability

The authors confirm that the data supporting the findings of this study are available within the article and its supplementary information (SI). Supplementary information is available. The Supplementary Information contains: Table S1 (Chemicals and materials used), Table S2 (Comparison with electrochemical and functionalized adsorbents), Fig. S1 (Reaction chemistry equation), Fig. S2 (Contact angle with water), Fig. S3 (PXRD of electrode products), and Fig. S4 (Effect of counter electrode size). See DOI: https://doi.org/10.1039/d5gc05411g.

Acknowledgements

This work was supported by the “Hundreds Talents Program” from the Chinese Academy of Sciences, Fujian Program for High-Level Entrepreneurial and Innovative Talents Introduction, the Double Thousand Plan of Jiangxi Province, the National Key R&D Program of China (2017YFE0106900), the Key R&D Program of Jiangxi Province (20203B BG72W013), and the Key Program of the Chinese Academy of Science (ZDRW CN-2021-3-1).

References

1 Y. Ghorbani, I. M. S. K. Ilankoon, N. Dushyantha and G. T. Nwaila, *Resour., Conserv. Recycl.*, 2025, **212**, 107966.
2 E. Alonso, A. M. Sherman, T. J. Wallington, M. P. Everson, F. R. Field, R. Roth and R. E. Kirchain, *Environ. Sci. Technol.*, 2012, **46**, 3406–3414.
3 Y. Wang, X. Chen, X. Hu, P. Wu, T. Lan, Y. Li, H. Tu, Y. Liu, D. Yuan, Z. Wu, Z. Liu and J. W. Chew, *Appl. Surf. Sci.*, 2021, **536**, 147829.
4 S. Ni, Y. Gao, G. Yu, S. Zhang, Z. Zeng and X. Sun, *J. Hazard. Mater.*, 2023, **460**, 132465.
5 M. Xu, W. Wang and D. Hua, *Adv. Funct. Mater.*, 2024, **34**, 2402130.
6 K. W. Chung, H. S. Yoon, C. J. Kim, J. Y. Lee and R. K. Jyothi, *J. Ind. Eng. Chem.*, 2020, **83**, 72–80.
7 N. T. Hung, L. B. Thuan, T. C. Thanh, M. Watanabe, D. V. Khoai, N. T. Thuy, H. Nhuan, P. Q. Minh, T. H. Mai, N. V. Tung, D. T. T. Tra, M. K. Jha, J. Y. Lee and R. K. Jyothi, *Hydrometallurgy*, 2020, **198**, 105506.
8 D. Talan and Q. Huang, *Minerals*, 2020, **11**, 20.
9 P. K. Vijayan, V. Shivakumar, S. Basu and R. K. Sinha, *Prog. Nucl. Energy*, 2017, **101**, 43–52.
10 S. Banerjee and H. P. Gupta, *Prog. Nucl. Energy*, 2017, **101**, 4–18.
11 J. Emblemsvåg, *Int. J. Sustainable Green Energy*, 2021, **41**, 514–537.
12 A. V. Colton and B. P. Bromley, *Nucl. Technol.*, 2018, **203**, 146–172.
13 G. Shakiba, R. Saneie, H. Abdollahi, E. Ebrahimi, A. Rezaei and M. Mohammadkhani, *J. Environ. Chem. Eng.*, 2023, **11**, 110777.
14 J. Su, Y. Gao, S. Ni, R. Xu and X. Sun, *J. Hazard. Mater.*, 2021, **406**, 124654.
15 W. B. Larrinaga, B. J. Lake, V. D. Pacanowski, M. G. Patterson, M. Hudson, F. M. Carlson, G. Heselschwerdt, S. Balboa, S. M. Biros and E. J. Werner, *Inorg. Chem.*, 2024, **63**, 13815–13819.
16 N. Azhar, K. M. Takip, R. Hazan, W. S. Paulus, N. A. Sapiee and J. Kones, IOP Conference Series: Materials Science and Engineering, MSE, 2020, vol. **785**, pp. 012015.
17 L. T. Sha, Q. Wu, Y. F. Zhang, W. J. Wang, F. Wu, Q. G. Huang and Z. Y. Yan, *Chem. Eng. J.*, 2024, **502**, 157841.
18 L. Xu, C. Xu, H. Bao, I. Spanopoulos, W. Ke, X. Dong, C. Xiao and M. G. Kanatzidis, *ACS Appl. Mater. Interfaces*, 2021, **13**, 37308–37315.
19 Y. Zhi, G. Duan, Z. Lei, H. Chen, H. Zhang, H. Tian and T. Liu, *Gels*, 2022, **8**, 378.
20 A. A. Alqadami, M. Naushad, Z. A. Alothman and A. A. Ghfar, *ACS Appl. Mater. Interfaces*, 2017, **9**, 36026–36037.
21 X. Chen, X. Liu, S. Xiao, W. Xue, X. Zhao and Q. Yang, *Sep. Purif. Technol.*, 2022, **297**, 121517.
22 W. Zhong, M. Wang, H. Hu, J. Qian, S. Wang, X. Su, S. Xiao, H. Xu and Y. Gao, *Sep. Purif. Technol.*, 2024, **347**, 127603.
23 X. Liu, S. Xiao, T. Jin, F. Gao, M. Wang, Y. Gao, W. Zhang, Y. Ouyang and G. Ye, *Sep. Purif. Technol.*, 2022, **296**, 121413.
24 X. H. Xiong, Y. Tao, Z. W. Yu, L. X. Yang, L. J. Sun, Y. L. Fan and F. Luo, *Chem. Eng. J.*, 2020, **384**, 123240.
25 S. Yang, Z. Luan, W. Li, X. Cheng, Z. Ye and B. Hu, *Sep. Purif. Technol.*, 2024, **330**, 125378.
26 J. Liao, T. Xiong, Z. Zhao, L. Ding, W. Zhu and Y. Zhang, *J. Cleaner Prod.*, 2022, **374**, 134059.
27 H. Zhang, C. Li, N. Wang, F. Jin, H. Liang, R. Wang, R. Guo, Z. Mo, W. Tian and N. Liu, *J. Environ. Chem. Eng.*, 2024, **12**, 111698.
28 N. Pan, L. Li, J. Ding, R. Wang, Y. Jin and C. Xia, *J. Colloid Interface Sci.*, 2017, **508**, 303–312.
29 C. Liu, P. C. Hsu, J. Xie, J. Zhao, T. Wu, H. Wang, W. Liu, J. Zhang, S. Chu and Y. Cui, *Nat. Energy*, 2017, **2**, 17007.
30 C. Wang, A. S. Helal, Z. Wang, J. Zhou, X. Yao, Z. Shi, Y. Ren, J. Lee, J. K. Chang, B. Fugetsu and J. Li, *Adv. Mater.*, 2021, **33**, 2102633.
31 T. Lin, T. Chen, C. Jiao, H. Zhang, K. Hou, H. Jin, Y. Liu, W. Zhu and R. He, *Nat. Commun.*, 2024, **15**, 4149.
32 J. G. Kim, H. B. Kim and K. Baek, *Sci. Total Environ.*, 2023, **886**, 163891.
33 Z. Dong, Z. Zhao, F. Wang, F. Wang and M. Xia, *Green Chem.*, 2023, **25**, 10576.
34 W. Tang, D. Li, X. Zhang, F. Guo, C. Cui, M. Pan, D. Zhang, J. Li and X. Xu, *Sep. Purif. Technol.*, 2023, **319**, 124087.
35 A. I. Wiechert, A. P. Ladshaw, L. J. Kuo, H. B. Pan, J. Strivens, N. Schlafer, J. R. Wood, C. Wai, G. Gill, S. Yiacoumi and C. Tsouris, *Ind. Eng. Chem. Res.*, 2020, **59**, 13988–13996.
36 J. Kim, C. Tsouris, Y. Oyola, C. J. Janke, R. T. Mayes, S. Dai, G. Gill, L. J. Kuo, J. Wood, K. Y. Choe, E. Schneider and H. Lindner, *Ind. Eng. Chem. Res.*, 2014, **53**, 6076–6083.
37 A. Kaygun and S. Akyil, *J. Hazard. Mater.*, 2007, **147**, 357–362.
38 K. Shao, G. Xu, X. Li, X. Liu, J. Han, H. Yang, G. Wang, Y. Guo and J. Dou, *Sep. Purif. Technol.*, 2025, **354**, 128822.
39 M. Pan, C. Cui, W. Tang, Z. Guo, D. Zhang, X. Xu and J. Li, *Sep. Purif. Technol.*, 2022, **281**, 119843.
40 X. Tang, Y. Liu, M. Liu, H. Chen, P. Huang, H. Ruan, Y. Zheng, F. Yang, R. He and W. Zhu, *Nanoscale*, 2022, **14**, 6285–6290.
41 J. Xiong, S. Hu, Y. Liu, J. Yu, H. Yu, L. Xie, J. Wen and X. Wang, *ACS Sustainable Chem. Eng.*, 2017, **5**, 1924–1930.
42 F. Liu, Z. Hu, M. Xiang and B. Hu, *Appl. Surf. Sci.*, 2022, **601**, 154227.
43 G. Cheng, A. Zhang, Z. Zhao, Z. Chai, B. Hu, B. Han, Y. Ai and X. Wang, *Sci. Bull.*, 2021, **66**, 1994–2001.
44 L. Xu, Y. Chen, W. Su, J. Cui and S. Wei, *Sep. Purif. Technol.*, 2023, **309**, 123024.
45 W. R. Cui, C. R. Zhang, W. Jiang, F. F. Li, R. P. Liang, J. Liu and J. D. Qiu, *Nat. Commun.*, 2020, **11**, 436.